

Underwater Time-of-Flight Camera for Remotely Operated Vehicle Applications

Evelyn S. DeMember
Tactical Systems Division
Physical Sciences Inc.
Andover, MA, USA

Andrew D. Bergey
Dept. of Elec. & Comp. Engr.
Grove City College
Grove City, PA, USA

Caleb J. Pipes
Dept. of Mech. Engr.
Grove City College
Grove City, PA, USA

Nathaniel H. Stuyck
Dept. of Mech. Engr.
Grove City College
Grove City, PA, USA

Luke K. Rumbaugh
Dept. of Elec. & Comp. Engr.
Grove City College
Grove City, PA, USA

David W. Illig
Warfighter Basic and Applied Research Division
NAWCAD
Patuxent River, MD, USA

Abstract—This paper describes recent developments in the use of a time-of-flight (ToF) camera for 3D imaging aboard underwater vehicles. We have modified a commercial camera for use underwater with green illuminators and have packaged and deployed this camera as payload aboard a BlueROV2. In this paper, we describe the system hardware, including the 525 nm laser diode illuminator modules, the signal breakout board, and the wide field of view optics. We also show imaging and ranging results from laboratory and field tests with the 3D camera and discuss the challenges introduced by absorption and scattering in turbid water. We show preliminary results from a method for improving imaging in turbid water via backscatter subtraction.

Index Terms—Underwater optics, time-of-flight, ToF cameras, oceanography, lasers, laser diodes

I. INTRODUCTION

Time-of-flight (ToF) cameras are finding many applications as 3D mapping, navigation, and modeling tools [1]–[3]. These cameras simultaneously generate amplitude and depth images by measuring both the reflectivity and distance of every pixel for every frame [4]. ToF cameras are particularly well suited for deployment on small vehicles because they provide video frame rates, centimeter depth resolution, and ambient light rejection, with low computational burden and a small footprint.

The goal of this project is to evaluate the use of ToF cameras as 3D imaging sensors underwater, with a particular focus on deployment aboard remotely operated vehicles (ROVs). The initial obstacle preventing underwater use is that most ToF sensors are designed to use infrared light, which is absorbed by water. Previous work on this project has demonstrated the use of green lasers and modified camera optics to allow underwater imaging [5]. Previous work has also shown the challenge of low signal-to-noise ratio (SNR) due to the low power density per pixel when using flood illumination [6]. In turbid water, this SNR problem worsens due to absorption, while range errors develop due to multi-path interference (MPI) from scattering particles [7], [8].

In this paper, we attempt to address the SNR problem by showing a path to scalable power via multiple modular illumination units, interfaced with the camera through a custom

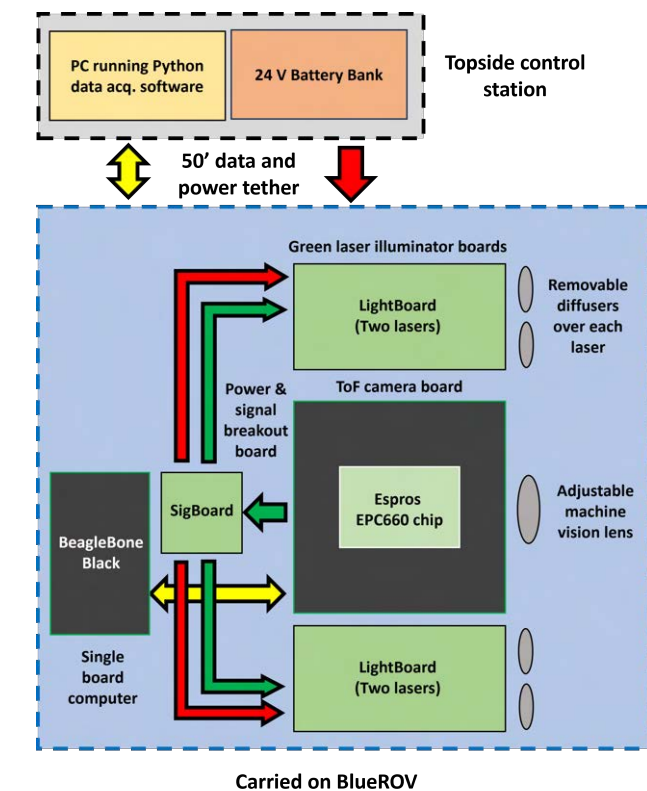


Fig. 1. ROV-mounted time-of-flight system block diagram. Connection arrows are color-coded by signal type: yellow for digital data, red for power flow, and green for laser timing.

signal routing board. We show imaging and ranging with multiple illumination modules. We next describe deployment of the system on an ROV for tests in turbid water in laboratory test tank and lake environments. Finally, we show promising preliminary results from applying a background subtraction method for reducing backscatter in the images [9].

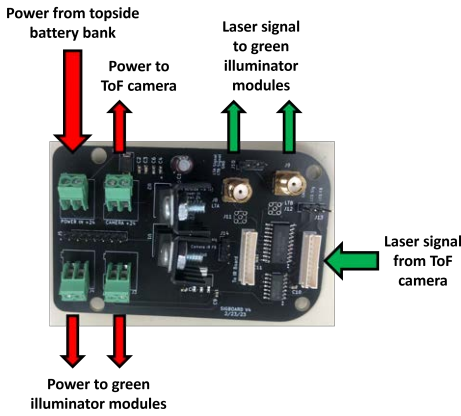


Fig. 2. SigBoard: Signal and power breakout board.

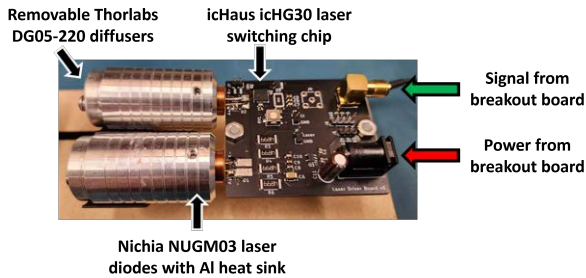


Fig. 3. LightBoard: Green laser illuminator board.

II. TOF CAMERA HARDWARE DESIGN

Figure 1 shows the block diagram of the ToF camera system. Our underwater ToF camera is built around an Espros EPC660 evaluation kit. The stock EPC660 kit uses infrared (IR) lasers for imaging and uses bursts of continuous-wave (CW) intensity modulation of up to 24 MHz. Since IR is quickly absorbed by water, we use green light instead of IR in order to use the EPC660 sensor underwater. To do this, we first removed the sensor’s IR filter and disabled the kit’s IR lasers. We then routed the camera’s laser drive signal through the “SigBoard” to two green laser illuminator “LightBoard” modules, each loaded with two 525 nm green lasers. We use the kit’s existing BeagleBone Black single-board computer with the Espros API to provide an Ethernet connection to the camera. Power and control of the camera are provided by a topside control station over a tether.

A. Camera module and signal routing board

Figure 2 shows the SigBoard PCB used to route the ≤ 24 MHz TTL laser drive signal to the two laser illuminator modules. The board breaks out the drive signal from the camera on its way to the built-in IR lasers. The signal is buffered and sent to the two illuminator modules. The board also routes power from the 24 V batteries to the camera, which runs on 24 V, and to the illuminator modules, which run on 12 V.

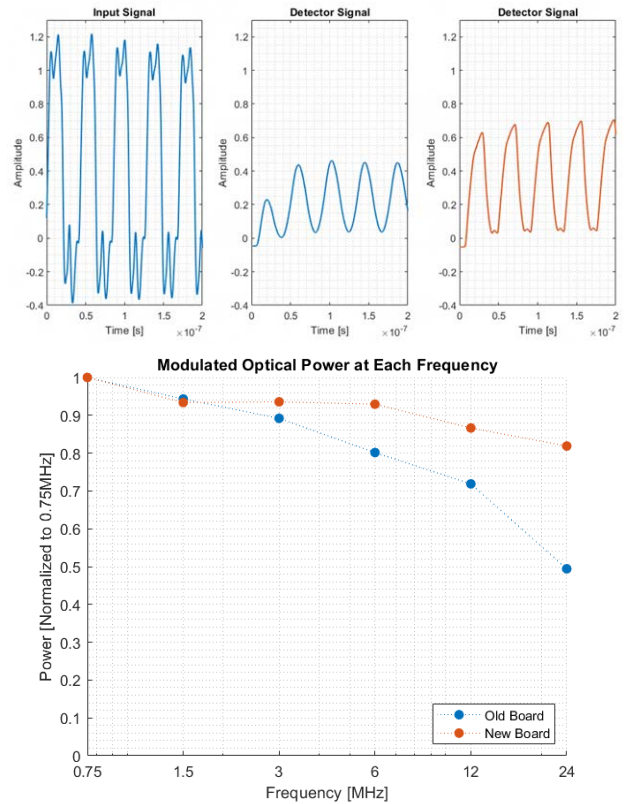


Fig. 4. Green laser illuminator intensity modulation produced by the new laser driver board. *Top*: Laser timing signals coming from ToF camera (left), and the resulting laser intensity modulation signals as recorded on a photodetector for the previous laser driver board (center) and the new board (right). *Bottom*: Frequency response of intensity modulation for the previous and new laser driver board, showing a 65% improvement in intensity modulation power at 24 MHz.

B. Illumination module and laser driver board

Each of the two illumination modules contains its own laser driver board. Figure 3 shows one of these LightBoards. Mounted to each driver board are two 1 W 525 nm Nichia NUGM03 green laser diodes. The diodes are fitted into aluminum heat sinks that carry removable diffusers. The board takes in a 0-5 V TTL laser drive signal from the signal routing board over a CAT6 cable. The driver board enables ≤ 24 MHz switching of the laser diodes at a peak current of ≤ 2 A and a duty cycle of 50% during each burst. The board is designed around the iC-Haus iC-HG30, a laser switching chip rated for ≤ 250 MHz switching speeds at ≤ 5 A CW current.

The LightBoard used in this system is an upgrade from an older version used in [6]. A problem observed in the older version was a decrease in the laser illuminators’ modulation depth as frequency increased. This is problematic because the higher frequencies allow better imaging quality and depth resolution. Use of the 24 MHz frequency could potentially improve imaging through backscatter in turbid water [10], [11]. Thus, this new board was designed to minimize trace impedance and laser current rise and fall time. Figure 4 shows the results of this redesign. The laser modulation

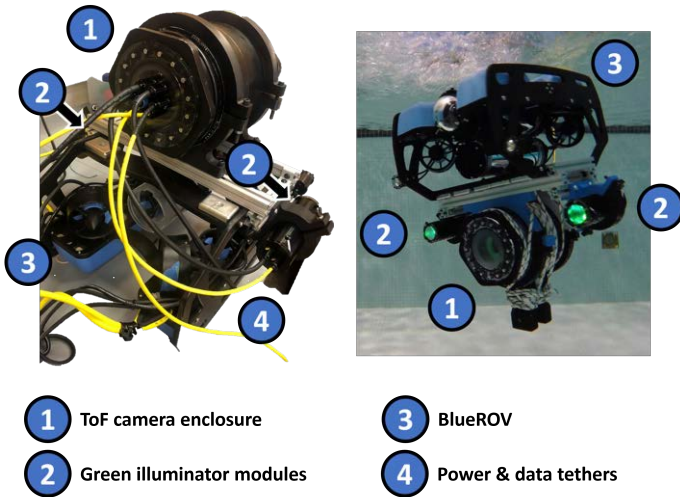


Fig. 5. ROV-mounted ToF camera system photos. *Left*: Benchtop assembly, with the BlueROV upside down. *Right*: ToF system deployed in pool.

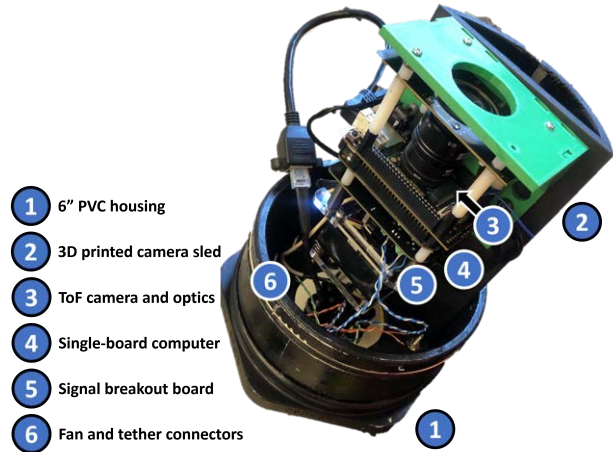


Fig. 6. Camera electronics tube.

was significantly improved at higher frequencies, showing a higher amplitude response compared to the old board. While improved, the signal integrity was still degraded and it still did not reach the desired flat frequency response.

C. Packaging and deployment on BlueROV2

The submersible packaging of the camera and illuminator modules is designed for deployment on a Blue Robotics BlueROV2, as shown in Figure 5. The camera stack, shown in Figure 6, is enclosed in a 6" PVC tube fitted with end caps containing laser-cut acrylic windows. This stack includes the Espros camera and its optics, the BeagleBone Black, the SigBoard, and a fan. The two illumination modules are attached to 3D-printed sleds inside of aluminum tubes and are mounted on either side of the camera enclosure. Blue Robotics Wetlink penetrators are used for all connections in and out of the tubes. A 50' twin power/data tether connects to the system to provide power and control the camera via Ethernet CAT6. Power is sourced from two 12 V batteries, and the camera communicates over TCP/IP with a Python data collection program running on the PC.

III. SYSTEM TESTING

A. Clear water testing in pool

The first field test of the ToF system deployed on the ROV was performed in a pool to establish a clear water benchmark. Depth accuracy was confirmed by the first test shown in Figure 7. In this experiment, a diver was positioned at varying distances away from the stationary camera. The diver moved throughout the full range of the camera operating at 24 MHz. (The upper limit of this range is constrained by the wavelength; exceeding the half-wavelength of the camera results in aliasing and thus inaccurate depth measurements.)

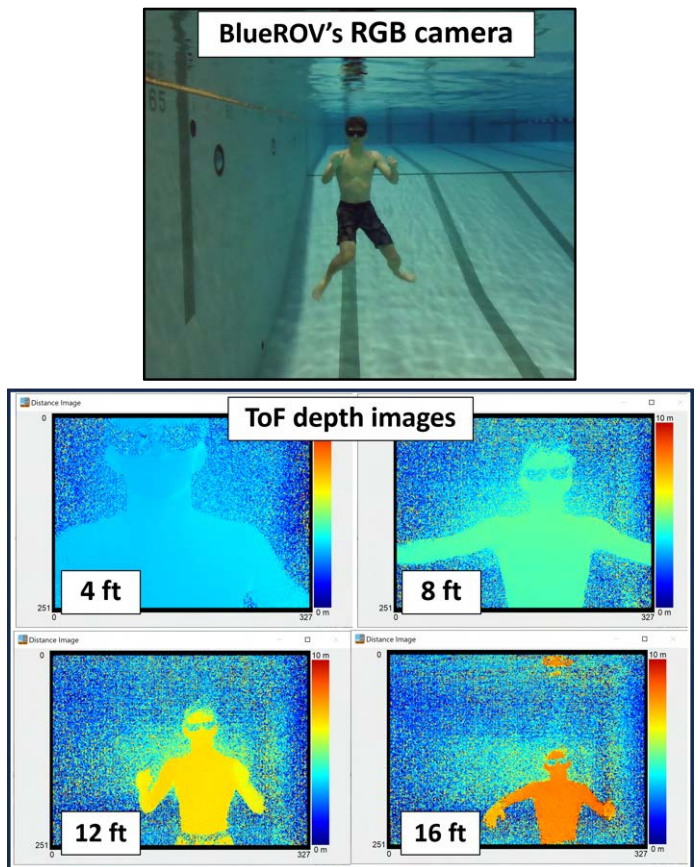


Fig. 7. Clear water images from testing in pool. *Top*: Establishing shot of swimmer with BlueROV's RGB camera. *Bottom*: Depth images taken with ToF camera at various distances. The swimmer's color changes with distance.

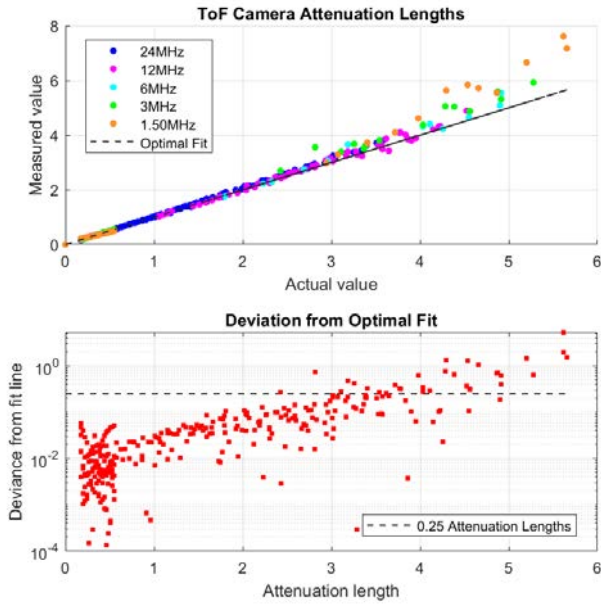


Fig. 8. Test of ToF camera’s distance accuracy trends while imaging a diffuse white object in increasingly turbid water. The illuminator modulation frequency is varied and the exposure time is fixed at 4 ms. *Top*: Measured distance versus actual distance of a single pixel on the object. *Bottom*: Error in distance measurements. The data trends show that all frequencies increase in error as turbidity increases. There are different slopes for different frequencies, perhaps indicating that backscatter’s effect differs with modulation frequencies.

B. Distance measurements as turbidity increases

Next, a more quantitative distance test was performed in a laboratory water tank. Images were taken of a diffuse white object in clear water, and the measured distance to the object was compared to the actual distance to the object. The turbidity of the water was then increased using liquid antacid [12].

Figure 8 shows the measured versus actual distance, where distance is given in attenuation lengths “ cz ”, *i.e.* the product of the distance z and the 532 nm exponential attenuation coefficient c of the water as measured by a Sea-Bird Scientific c -star transmissometer. Images were taken across the modulation frequency range of the camera. The distance measurements indicate that the camera is accurate in clear water but as the turbidity of the water increases, the error of the measurement increases steadily.

C. Turbid water testing in lake

A field test was also performed in which we attempted to image a Secchi disk in a highly turbid lake to get another view of the effects of backscatter. Figure 9 shows the experimental setup and some resulting amplitude imagery. In highly turbid water the images were dim because of attenuation. As we increased the exposure time, more light was collected and the Secchi disk’s pattern appeared. However after a certain point there was no advantage to collecting more light since the light was so heavily scattered by suspended particles. In this scatter-

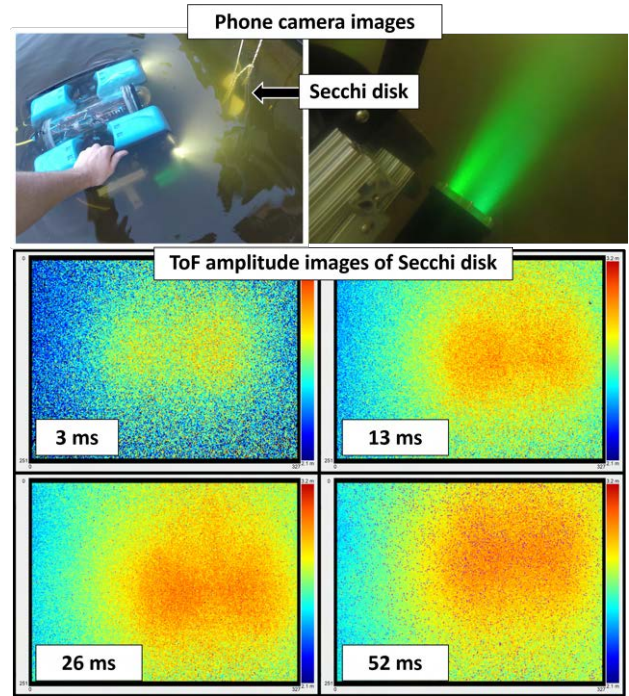


Fig. 9. Turbid water images from testing in lake. *Top*: Establishing shot of system on ROV imaging a Secchi disk through turbid water. *Bottom*: Amplitude images taken with ToF camera at various exposure times. The performance initially improves with increased exposure times, but then does not improve, showing that the imaging is scatter-limited.

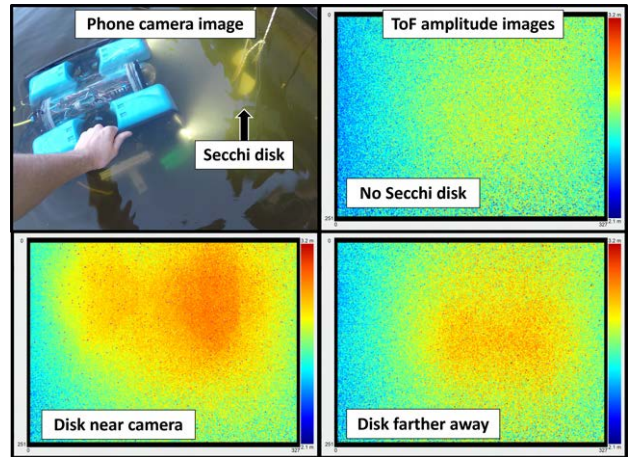


Fig. 10. Scatter-limited imaging in turbid water. *Top left*: Establishing shot of system on ROV imaging a Secchi disk. *Top right*: ToF camera amplitude image when Secchi disk is removed. This image is only backscatter. *Bottom left*: Amplitude image when Secchi disk is placed at 3’ away. The object region appears farther away (redder) than the backscatter, since the object is behind the center of the volumetric backscatter. *Bottom right*: Amplitude image when Secchi disk is placed at 4’ away. The object region appears closer than it did at 3’ away, since the distant object’s return is now weaker relative to the closer backscatter.

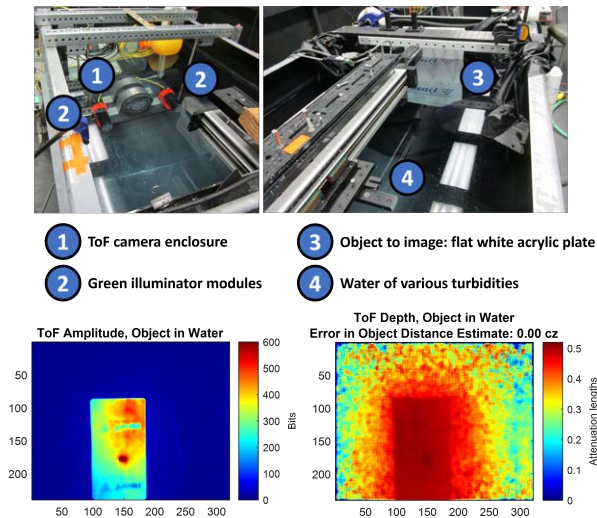


Fig. 11. Experimental setup for backscatter subtraction testing. *Top*: The ToF camera is submerged in a water tank and used to image a flat plate through water of various turbidities. *Bottom left*: Baseline ToF amplitude image of the object in clear water. *Bottom right*: Baseline ToF depth image of the object. The clear water measured distance to the object matches manual measurements and is considered ground truth.

limited environment the object is blurred by forward scatter and veiled by backscatter.

Figure 10 shows a second sequence of amplitude images from the same lake field test. These images demonstrate the MPI effect that is well known in the ToF literature [7], [8]. In this case, the return from the object and the return from the backscatter sum at each pixel. When the object return is strong, as in the image of the disk close to the camera, the object return dominates and the Secchi disk pattern is visible (albeit blurred). When the object return is weaker, the backscatter return dominates and the Secchi disk pattern is not clear. Moreover, the distance measured is actually *closer* to the ToF camera when the object moves away, because the camera is primarily measuring the distance to the backscatter. This shows how the ToF depth measurement can be thought of as a weighted sum of the backscatter and object measurements.

IV. BACKSCATTER REMOVAL

It was shown in [9] that homogeneous, statistically stationary backscatter in turbid water could be treated as a competing clutter “object” interfering with submerged objects, and could be removed to a large extent using a phasor backscatter subtraction method [7], [8]. We performed a laboratory water tank experiment with the ToF camera to investigate the effectiveness of this approach. Figure 11 shows the experimental setup for imaging a flat white object in a water tank. The turbidity was varied from clear water to harbor-like conditions using liquid antacid. The clear water images were validated by manual measurement and then used as a baseline ground truth for the following turbid water experiments. Figure 12 shows an example of the improvement when backscatter subtraction was used when the object was 4 cz from the camera. Before

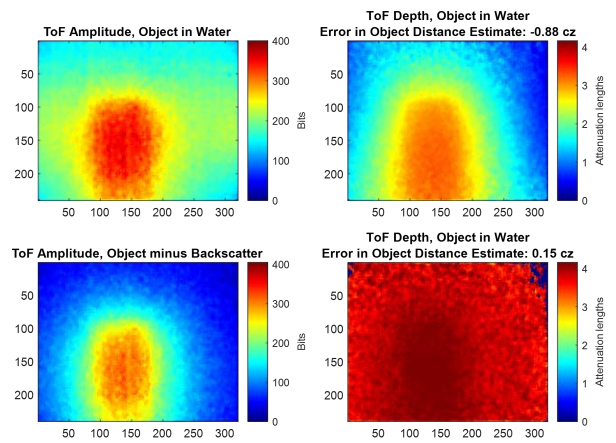


Fig. 12. Background subtraction for ToF images at 4 attenuation lengths. *Top left*: ToF amplitude, uncorrected. The object is blurred but clearly visible. Backscatter is emerging on the sides of the image. *Top right*: ToF depth, uncorrected. The blurred object is clear but the distance is skewed towards the camera by almost 1 cz. *Bottom left*: ToF amplitude, corrected. The object is blurred but visible. *Bottom right*: ToF depth, corrected. The depth estimate of the object is much closer to the ground truth.

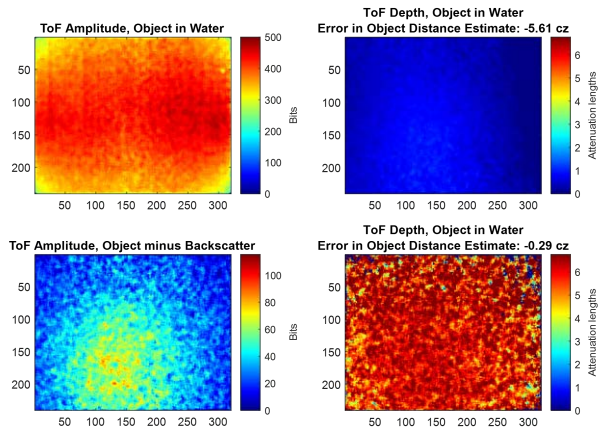


Fig. 13. Background subtraction for ToF images at 6.5 attenuation lengths. *Top left*: ToF amplitude, uncorrected. The object is no longer visible behind the backscatter. *Top right*: ToF depth, uncorrected. The blurred object may still be visible but the distance is skewed towards the camera by over 5 cz. *Bottom left*: ToF amplitude, corrected. The object is visible once the backscatter is removed. *Bottom right*: ToF depth, corrected. The depth estimate of the object remains close to the ground truth.

correction, the ToF depth measurement was nearly 1 cz closer than the clear water ground truth. After correction, the measurement was a reasonable match for the ground truth since the backscatter’s contribution was largely gone. Figure 13 shows a more extreme example in which the object is 6.5 cz from the camera. Here, correction allows the target to be seen “through” the backscatter in the ToF amplitude measurement. The uncorrected ToF depth measurement had an error of over 5 cz, but this was reduced to 0.3 cz after correction. Thus, the correction should improve both object detection and ranging.

V. CONCLUSIONS

In this paper we have described a ToF camera customized for underwater work and packaged for deployment aboard an ROV. We have shown pool, lake, and laboratory tests with this camera. We have demonstrated the camera's basic functionality, including accurate ranging in clear water. We have attempted to provide some insight into the challenges that emerge when operating in turbid water. Specifically, we have shown that the initial problem of attenuation-limited imaging can be addressed by multiple laser illuminators and longer exposure times. We then showed that scatter-limited ToF imaging can be thought of in terms of a weighted sum of the backscatter and the veiled objects. Based on this insight we demonstrated one path to scatter mitigation through background subtraction. This approach allowed for object detection and ranging at up to 6.5 attenuation lengths.

ACKNOWLEDGMENT

The authors thank William Jemison for loaning us the EPC660 camera kit, Austin Jantzi for discussions on the backscatter removal approach, and Nick Sparks for assistance with the camera software driver. Riley Truitt and Alex Smith programmed the image acquisition software used for some of the field test experiments. *NAVAIR Public Release 2023-340 Distribution Statement A: Approved for public release; distribution is unlimited.*

REFERENCES

- [1] T. Oggier, B. Büttgen, F. Lustenberger, G. Becker, B. Rüegg, and A. Hodac, "SwissRanger SR3000 and first experiences based on miniaturized 3D-TOF cameras." Proc. of the First Range Imaging Research Day at ETH Zurich, Sept. 2005.
- [2] M. Hansard, L. Seungkyu, C. Ouk, and R. P. Horaud Time-of-flight cameras: principles, methods and applications. Springer Science and Business Media, 2012.
- [3] M. Stefan, D. Dr'oschel, S. Fuchs, D. Holz, and A. Nüchter, "Robust 3D-mapping with time-of-flight cameras." Proc. of 2009 IEEE/RSJ International Conference on Intelligent Robots and Systems, pp. 1673—1678, October 2009.
- [4] L. Li, "Time-of-Flight Camera—An Introduction". Texas Instruments technical white paper, Literature No. SLOA190B 10, May 2014.
- [5] K. Mack, P. Athavale, W. Jemison, D. Illig, L. Rumbaugh, M. Banavar, and E. Bollt, "Restoration of time-of-flight (ToF) underwater images using TV regularization." Ocean Sensing and Monitoring XIII (Vol. 11752), pp. 128–135, SPIE, April 2021.
- [6] L. Rumbaugh, J. Will, J. Thomson, W. Jemison, and D. Illig, "Experiments using a 525 nm time-of-flight camera for object imaging and ranging in clear and turbid water." Ocean Sensing and Monitoring XIV (Vol. 12118), pp. 120–131 SPIE, May 2022.
- [7] N. Naik, A. Kadambi, C. Rhemann, S. Izadi, R. Raskar, and S. Bing Kang, "A light transport model for mitigating multipath interference in time-of-flight sensors." Proc. of IEEE Conference on Computer Vision and Pattern Recognition, pp. 73–81, June 2015.
- [8] K. Yamazaki, "Analysis of Phasor Distortions by Fog in Time-of-Flight Measurement". Thesis, University of Tsukuba, March 2020.
- [9] A. Jantzi, W. Jemison, P. Athavale, M. Banavar, E. Bollt, L. Rumbaugh, and D. Illig, "Underwater Time of Flight Camera Ranging with Backscatter Phasor Subtraction. Proc. of IEEE OCEANS 2022, Hampton Roads, VA, pp. 1–7, Oct. 2022.
- [10] L. Mullen and V. Contarino, "Hybrid LIDAR-radar: Seeing through the scatter". IEEE Microwave Magazine vol. 1.3, pp. 41–48, 2000.
- [11] F. Pellen, X. Intes, P. Olivard, Y. Guern, J. Cariou, J. Lotrian, "Determination of sea-water cut-off frequency by backscattering transfer function measurement". Journal of Physics D: Applied Physics vol. 33.4, pp. 349–354, 2000.
- [12] L. Mullen, D. Alley, and B. Cochenour, "Investigation of the effect of scattering agent and scattering albedo on modulated light propagation in water". Applied Optics vol. 50.10, pp. 1396–1404, 2011.